

Modular fabrication of fluorescent sensors via hydrogen-bonding self-assembly



Qian Zhang, Yuhan Huang, Yuemin Wang, Shunhua Li*, Yunbao Jiang

Department of Chemistry and the MOE Key Laboratory of Spectrochemical Analysis & Instrumentation, College of Chemistry and Chemical Engineering, Xiamen University, Xiamen, 361005, China

ARTICLE INFO

Keywords:

Modularization
Fluorescent chemosensors
Hydrogen-bonding self-assembly
Noncovalent synthesis

ABSTRACT

Fluorescent molecular sensors offer a sensitive and straightforward approach to monitoring biologically or environmentally important targets. However, obtaining high-performance chemosensors are still challenging in terms of laborious synthesis and low success rate. Herein we report a general and efficient strategy for fabrication of complex fluorescent chemosensors. Noncovalent synthesis of supramolecular sensors was realized by self-assembly of structurally simple subunits bearing hydrogen-bonding linkers. Based on the selected use of three recognition subunits and three signalling subunits, an array of fluorescent sensory co-assemblies with different subunits combination patterns were fabricated for sensitive detection of bisulfite, saccharides, carbon dioxide or chemical warfare agents. The multiplicity and ratios of these subunits can be flexibly adjusted to obtain desirable functions such as signal amplification, ratiometric responses and simultaneous multitarget monitoring.

1. Introduction

Fluorescent molecular sensors or probes offer a powerful tool for exploring biological or environmental systems in terms of high sensitivity, multiple parameters (e. g. intensity, lifetime, anisotropy, emission wavelength, etc.), and possibility of real-time and real-space monitoring [1–6]. In fabricating the sensors, high-performance luminophores should be finely connected to the target-specific recognition groups in order to obtain sensitive and reliable fluorescence responses [7–9]. It is not hard to imagine that laborious synthesis is generally involved in constructing a novel fluorescent chemosensor (FCS). Although FCSs of an ever-increasing diversity have been developed for cations [10–15], anions [16–19], gasotransmitters [20–25], reactive oxygen species [26–30], and other species of biological or environmental interest [31–41], there is no general strategy for fabrication of FCSs. In addition, FCSs with complex structure and function are greatly undeveloped because of the challenges in both design and synthesis.

Generally, FCS is composed of at least one recognition subunit which is responsible for binding the target and one signalling subunit which displays fluorescence change upon target binding. In most cases, covalent coupling of these subunits is adopted in developing FCSs, leading to a low degree of flexibility in the control of molecular structure. If the recognition and signalling subunits can be synthesized separately and flexibly self-assembled into sensory supramolecules,

modular fabrication of FCSs might be realized. This new fabrication concept offers a general approach with obvious merits to develop FCSs. Firstly, synthesis difficulty of the sensors remarkably decreases. Secondly, the recognition and signalling subunits can be easily varied in a combinatorial manner to serve different sensing targets or signalling patterns. Thirdly, the multiplicity and ratios of the subunits can be flexibly adjusted to obtain desirable sensing performances. However, it is necessary to support such a noncovalent fabrication strategy by an efficient self-assembly platform to enable the reversible and specific incorporation of programmable subunits [42]. Current strategy pioneered by König et al. is basing modular chemosensors on non-covalent embedding of amphiphilic subunits into vesicle membranes [43]. The fluidity of vesicle membranes makes the subunits weakly addressable, and seeking for alternative platforms to make subunit combination more controllable is still an important task.

Our method is to fabricate sensory supramolecules via hydrogen-bonding (HB) self-assembly of the sensing subunits which are functionalized with suitable HB linkers (Fig. 1). Indeed, “noncovalent synthesis” using HB has proven to be an efficient approach to fabrication of complex but well-defined structures that combine flexibility with practicality [42,44]. However, this alternative strategy to covalent synthesis has never been applied to the construction of sensory supramolecules with a same degree of structural complexity and/or functionality. In our study, the HB linkers were designed to integrate at least

* Corresponding author.

E-mail address: lishua@xmu.edu.cn (S. Li).

<https://doi.org/10.1016/j.dyepig.2019.05.011>

Received 13 March 2019; Received in revised form 6 May 2019; Accepted 6 May 2019

Available online 10 May 2019

0143-7208/ © 2019 Elsevier Ltd. All rights reserved.

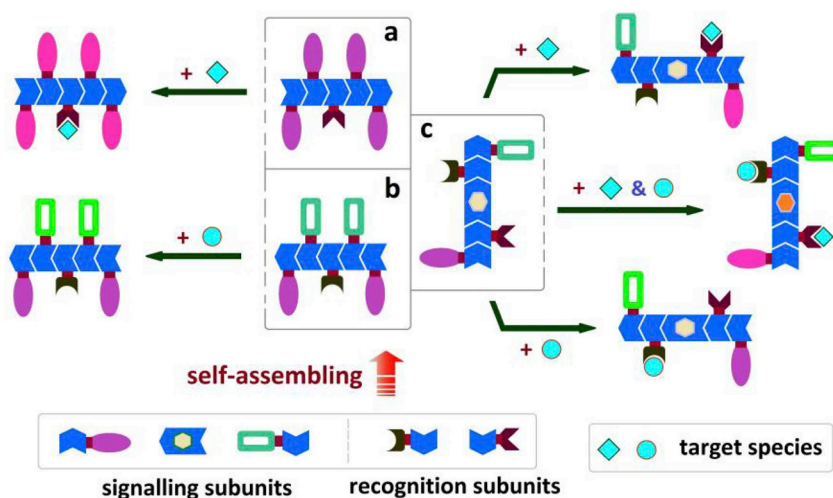


Fig. 1. Schematic representation of fluorescent supramolecular sensors with different subunits combination patterns. a, Sensory supramolecules self-assembled from unitary recognition subunits with unitary signalling subunits. b, Sensory supramolecules self-assembled from unitary recognition subunits with binary signalling subunits. c, Sensory supramolecules self-assembled from binary recognition subunits with ternary signalling subunits. These three sensing patterns are associated with the easy realization of signal amplification (a), ratiometric responses (b) and simultaneous multitarget monitoring (c), respectively.

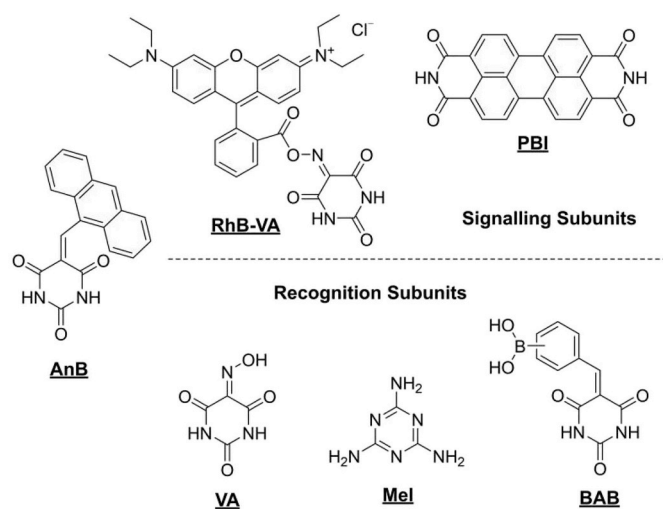


Fig. 2. The recognition and signalling subunits investigated in this study.

two donor-acceptor-donor (DAD) or acceptor-donor-acceptor (ADA) HB-active sites into a rigid and planar framework (Fig. 2). Some small-molecule chemicals such as barbituric acid fit this purpose well and can be easily grafted with luminophores or target-binding moieties to give the signalling or recognition subunits, respectively. Because of the high self-assembling tendency of the HB linkers [45–47], ordered and elastic aggregates of the subunits can be easily formed in aqueous or organic solutions as a bran-new type of sensing systems. Upon interacting with the target species, the binding-induced conformation change is ready to extend to the whole sensory aggregates through reorganization of the HB networks to result in sensitive fluorescence responses. On the other hand, the dynamic connection between the subunits enables flexible variation of the subunit combination pattern to meet different sensing purposes (Fig. 1).

2. Experimental

2.1. General remarks

All syntheses of the subunits were performed under a nitrogen atmosphere using standard Schlenk techniques, unless otherwise stated.

Acetone was distilled from calcium sulfate immediately before use. Other reagents were used as received from commercial sources without further purification. AnB was synthesized as we previously reported [48]. Column chromatography was performed on alumina gel (200–300 mesh) in air.

Absorption and fluorescence spectra were recorded on a Hitachi U-3900 ultraviolet–visible spectrophotometer and a Hitachi F-7400 fluorophotometer, respectively. Electrospray ionisation (ESI) mass spectra were recorded on a Bruker ESQUIRE-3000⁺ mass spectrometer. The nuclear magnetic resonance (NMR) experiments were performed on a Bruker Avance II 400 MHz NMR spectrometer. ¹H and ¹³C NMR chemical shifts (δ) are relative to tetramethylsilane. The absolute values of the coupling constants are given in Hertz (Hz). Multiplicities are abbreviated as singlet (s), doublet (d), triplet (t), multiplet (m) and broad (br). The dynamic light scattering (DLS) data were collected from a Malvern Zetasizer Nano-zsMPT-2 particle size and zeta potential analyzer. Infrared spectra were recorded on a Nicolet AVATAR FT-IR 360 spectrophotometer. Morphologic evolutions of the self-assemblies were studied by a Tecnai G2 Spirit BioTwin transmission electron microscope.

2.2. Synthesis and characterization of RhB-VA

To a solution of rhodamine B (0.50 g 1.1 mmol) in acetone (15 mL) at room temperature, 2.0 mL phosphorus(V) oxychloride was added dropwise under vigorous agitation. The mixture was then refluxed under nitrogen atmosphere for about 5 h. The product was dried under vacuum and redissolved in dried acetone (15 mL). In a 50 mL two-neck flask, a solution of violuric acid (VA) monohydrate (106 mg, 0.6 mmol) in acetone (15 mL) was stirred at -5°C (in an ice-salt bath) for 40 min. The solution of the acyl chloride product of rhodamine B was added dropwise to the cooled solution of VA and the resulting mixture was stirred overnight at room temperature. The reaction mixture was concentrated under reduced pressure. The residue was further purified by column chromatography (silica gel; 2.5% MeOH/CH₂Cl₂, V/V). Yield: 22 mg, 21%. The selected spectroscopic data of RhB-VA are as follows. FT-IR (KBr, cm⁻¹): ν_{max} = 3505 (N–H), 3178 (HB-related N–H), 3060 and 2805 (C–H), 1722 and 1712 (C=O), 1685 (C=N), 1431 and 1331 (HB-related C=O). ¹H NMR (400 MHz, DMSO-*d*₆, ppm): δ = 11.42 (s, 1H, NH), 11.31 (s, 1H, NH), 8.23 (d, 1H, *J* 7.6, ArH), 7.86 (t, 1H, *J* 6.8, ArH), 7.81 (t, 1H, *J* 7.2, ArH), 7.41 (d, 1H, *J* 7.2, ArH), 7.10 (d, 2H, *J* 10.8, ArH), 7.02–6.97 (m, 4H, ArH), 3.65 (q, 8H, *J* 6.9, NCH₂CH₃), 1.21

(t, 12H, J 7.0, NCH_2CH_3). ^{13}C NMR (100 MHz, $\text{DMSO}-d_6$, ppm): δ = 166.73, 159.57, 159.16, 157.57, 155.53, 150.16, 136.63, 133.61, 133.12, 131.45, 131.40, 130.81, 130.67, 114.94, 113.36, 96.32, 52.92, 49.06, 45.8, 12.9. ESI-MS: m/z calcd for $[\text{C}_{32}\text{H}_{32}\text{N}_5\text{O}_6]^+$, 582.63; found, 582.7.

2.3. Synthesis and characterization of BAB

A mixture of barbituric acid (328 mg, 2 mmol) and glacial acetic acid (10 mL) in deionized water (20 mL) was heated to give a colorless solution. 4-Formylphenylboronic acid (300 mg, 2 mmol) was added in this solution and the resulting mixture was refluxed under nitrogen atmosphere for two days to give a yellow precipitate. The solid was collected by filtration, washed with methanol and dried under vacuum. Yield: 262 mg, 89%. The selected spectroscopic data of *para*-BAB are as follows. FT-IR (KBr, cm^{-1}): ν_{max} = 3478 (O–H), 3360 (N–H), 3251 (HB-related N–H), 3050 and 2860 (C–H); 1749 and 1676 (C=O), 1376 and 1322 (HB-related C=O). ^1H NMR (400 MHz, $\text{DMSO}-d_6$, ppm): δ = 11.43 (s, 1H, NH), 11.23 (s, 1H, NH), 8.28 (s, 1H, CH), 8.24 (m, 2H, BOH), 7.99 (d, 2H, J 8.0, ArH), 7.85 (d, 2H, J 8.0, ArH). ^{13}C NMR (100 MHz, $\text{DMSO}-d_6$, ppm): δ = 163.84, 161.98, 155.12, 150.66, 134.48, 133.95, 132.21, 119.79. ESI-MS: m/z calcd for $[\text{C}_{11}\text{H}_8\text{BN}_2\text{O}_5]^-$, 259.00; found, 259.01.

Similar synthesis procedure was followed with 2-formylphenylboronic acid or 3-formylphenylboronic acid to obtain *ortho*- or *meta*-BAB, respectively. Addition of glacial acetic acid was not needed in synthesis of *ortho*-BAB.

The selected spectroscopic data of *ortho*-BAB are as follows. FT-IR (KBr, cm^{-1}): ν_{max} = 3558 (O–H), 3496 (N–H), 3201 (HB-related N–H), 3041 and 2854 (C–H); 1752 and 1671 (C=O), 1420 and 1358 (HB-related C=O). ^1H NMR (400 MHz, $\text{DMSO}-d_6$, ppm): δ = 11.37 (s, 1H, NH), 11.22 (s, 1H, NH), 8.27 (s, 1H, CH), 8.18 (m, 2H, ArH), 7.93 (d, 1H, J 6.0, ArH), 7.45 (t, 1H, J 6.4, ArH). ^{13}C NMR (100 MHz, $\text{DMSO}-d_6$, ppm): δ = 163.90, 162.05, 155.72, 150.83, 140.07, 138.34, 134.45, 132.30, 127.66, 119.26. ESI-MS: m/z calcd for $[\text{C}_{11}\text{H}_{10}\text{BN}_2\text{O}_5]^+$, 261.02; found, 261.1.

The selected spectroscopic data of *meta*-BAB are as follows. FT-IR (KBr, cm^{-1}): ν_{max} = 3533 (O–H), 3424 (N–H), 3223 (HB-related N–H), 3045 and 2857 (C–H); 1750 and 1678 (C=O), 1392 and 1338 (HB-related C=O). ^1H NMR (400 MHz, $\text{DMSO}-d_6$, ppm): δ = 11.38 (s, 1H, NH), 11.23 (s, 1H, NH), 8.27 (s, 1H, CH), 8.18 (m, 2H, ArH), 7.91 (d, 1H, J 7.6, ArH), 7.45 (d, 1H, J 8.4, ArH). ^{13}C NMR (100 MHz, $\text{DMSO}-d_6$, ppm): δ = 163.89, 162.00, 155.73, 150.70, 140.06, 138.35, 134.46, 132.31, 127.65, 119.25. ESI-MS: m/z calcd for $[\text{C}_{11}\text{H}_8\text{BN}_2\text{O}_5]^-$, 259.00; found, 259.6.

3. Results and discussion

3.1. Design of the recognition and signalling subunits

Because of the DAD-type HB activity of imide, planar bisimides were employed as HB linkers with high tendency to self-assemble into HB polymers [46]. Barbituric acid and violuric acid, both of which contain a bisimide-integrated six-membered ring, were grafted onto 9-anthraldehyde and rhodamine B to give the signalling subunits **AnB** and **RhB-VA**, respectively (Fig. 2). In both cases, the fluorophores exist as the side chains of the resulting HB polymers after self-assembly of the subunits. However, different from anthracene which is ready to display monomer/excimer dual emission change, rhodamine B usually undergoes fluorescence quenching upon aggregation. Perylene bisimide (**PBI**) was selected as another signalling subunit whose fluorophore will be inserted into the HB polymer backbones during self-assembling and display remarkably aggregation-dependent fluorescence changes

because of its high π - π stacking tendency. The fluorescence emissions from these three signalling subunits almost cover the whole visible region and can be distinguished by different colours. In addition, each two of the three fluorophores can be excited simultaneously to induce ratiometric emissions.

Based on a similar motif of HB linkers, recognition subunits aiming for different sensing targets were developed. The interaction between boronic acid and diols has been widely applied to sensing saccharides [49,50]. Therefore, barbituric acid was treated with formylphenylboronic acid to obtain the saccharide recognition subunit **BAB**. **VA** and melamine (**Mel**) can be directly used as recognition subunits by taking advantage of the high affinity of oximes toward nerve agents and the Lewis acid-base interaction between amines and carbon dioxide [51,52], respectively. In the latter case, **Mel** itself is an efficient HB linker with triple ADA HB-active sites integrated in a planar six-membered ring. It is worth noting that in some cases barbituric acid itself can be used as a recognition subunit if the facile reaction between carbonyl and bisulfite is taken into account.

3.2. Sensory co-assemblies with unitary recognition subunits and unitary signalling subunits

A simple bisulfite sensing system based on **AnB** was first investigated to validate the self-assembly of barbituric acid linker and the signal transmission function of the resulting HB networks. Absorption spectra reveal the occurrence of pH-dependent aggregation of **AnB** in aqueous solution (Supplementary Fig. S1). At pH 7.0, the average diameter of the self-assemblies is about 450 nm in aqueous solution of 10 μM **AnB**. Because of carbonyl-bisulfite interaction and the resulting destruction of the DAD HB motif of **AnB** (Supplementary Fig. S3), the aggregation degree decreases dramatically after reaction with bisulfite (Supplementary Figs. S4 and S5). Consequently, addition of bisulfite induces a remarkable reduction of the anthracene excimer emission (at 513 nm) along with an enhancement of the anthracene local emission (at 413 nm) (Fig. 3A). No fluorescent response has been observed in the presence of other common anions. Taking advantage of the selective response, ratiometric fluorescent detection of bisulfite at the micromolar concentration level can be established (Fig. 3B), suggesting its applicability to sensing sulfur dioxide which has caused much environmental and physiological concern [53,54]. For example, this method has been applied to detection of sulfite residues in several samples of preserved fruits or pickles. There were no significant differences between the results obtained by our method and those by classic tetrachloromercurate-pararosaniline method (Supplementary Table S1).

To exemplify a more generalized sensing pattern based on unitary recognition subunits and unitary signalling subunits, the co-assemblies of **Mel** and **RhB-VA** were investigated for sensing CO_2 . Addition of **Mel** greatly enhances the aggregation of **RhB-VA** in DMF because of the strong DAD-ADA HB coupling. As a consequence, the **RhB-VA** dominated fluorescence (at 595 nm) is remarkably quenched (Fig. 3C). Upon interacting with CO_2 , the fluorescence is restored, whereas the co-assemblies show no fluorescence response toward other inorganic gases such as O_2 , N_2 and CO . This is attributed to the fact that CO_2 is able to destroy the HB coupling between **Mel** and **RhB-VA** by reaction with the amine groups of **Mel**. The described aggregation and disaggregation processes were confirmed by DLS tests (Supplementary Fig. S8). Importantly, the molar ratio of the subunits can be finely adjusted to modulate the sensitivity of the sensory co-assemblies. In this CO_2 sensing case, the signalling to recognition subunit ratio (S/R) was optimized at 5 (Fig. 4), indicating a signal amplification effect. Under the optimized conditions, sensitive fluorescent sensing of CO_2 can be carried out (Fig. 3D).

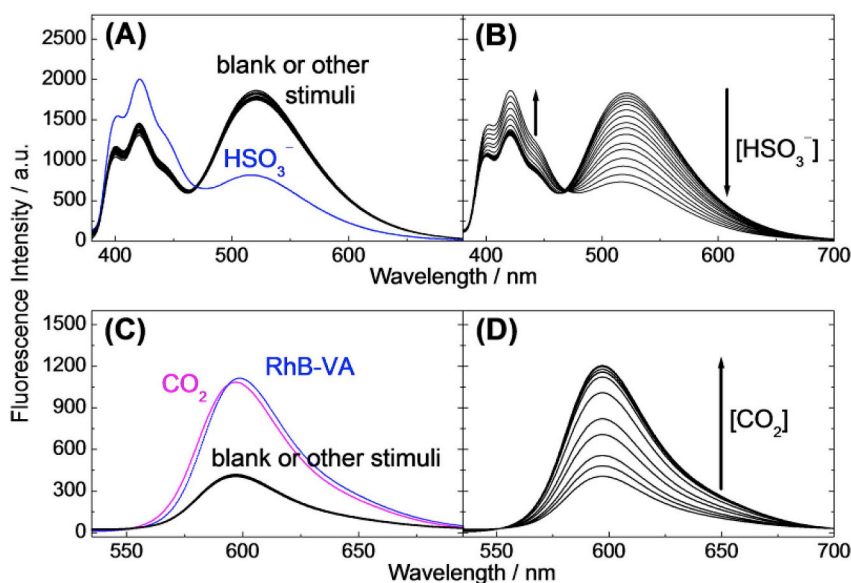


Fig. 3. Fluorescent responses of the investigated sensory assemblies with unitary recognition subunits and unitary signalling subunits. (A) Fluorescence responses of the self-assemblies of **AnB** (10 μM) to HSO_3^- (100 μM) or other anions (sodium salts, 1.0 mM) including CH_3COO^- , HCO_3^- , $\text{C}_2\text{O}_4^{2-}$, NO_2^- , NO_3^- , S^{2-} , $\text{S}_2\text{O}_3^{2-}$ and SO_4^{2-} in DMF/ H_2O (2:8, V/V) mixture buffered at pH 7.0 by 0.02 M NaH_2PO_4 – Na_2HPO_4 . (B) Fluorescence traces of the self-assemblies of **AnB** (10 μM) in the presence of increasing amount of NaHSO_3 (0, 5.0, 10, 20, 30, 40, 50, 60, 70, 80, 90, 95, 100 μM) in DMF/ H_2O (2:8, V/V) mixture buffered at pH 7.0 by 0.02 M NaH_2PO_4 – Na_2HPO_4 . (C) Fluorescent responses of the sensory co-assemblies of **Mel** and **RhB-VA** to different gases including CO_2 , O_2 , N_2 and CO in DMF. The concentrations of **RhB-VA** and **Mel** were kept at 50 μM and 10 μM , respectively. The spectrum of **RhB-VA** at the same concentration was inserted for a comparison. (D) Fluorescence traces of the sensory co-assemblies of **Mel** and **RhB-VA** in DMF upon bubbling with CO_2 for increasing time (0, 0.5, 1.0, 2.0, 3.0, 4.0, 5.0, 6.0, 7.0, 8.0, 9.0, 10 min). Excitation wavelengths: 371 nm for A and B; 526 nm for C and D.

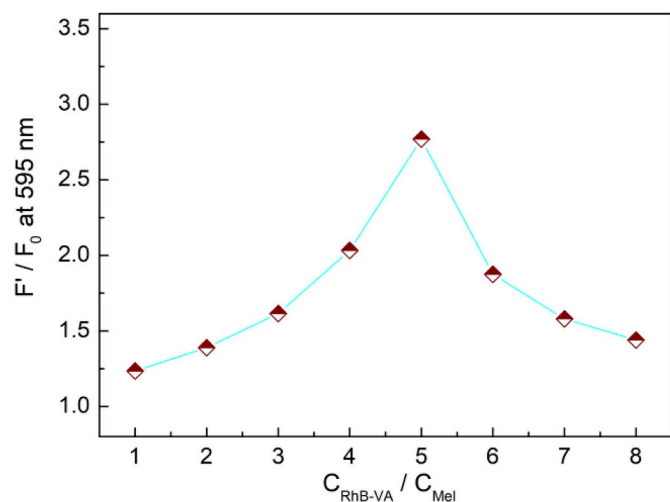


Fig. 4. Influence of the molar ratio of **RhB-VA** to **Mel** (10 μM) on the fluorescence response of [**Mel** + **RhB-VA**] sensory co-assemblies to CO_2 in DMF. $\lambda_{\text{ex}} = 526 \text{ nm}$. F_0 and F' are the emission intensity before and after interaction with CO_2 , respectively.

3.3. Sensory co-assemblies with unitary recognition subunits and binary signalling subunits

Without additional processing, different signalling subunits can be simultaneously involved in co-assembly with recognition subunits to result in ratiometric fluorescence responses, which support high reliability in quantification [27,55–57]. This fabrication pattern was first validated by a new sensing system for nerve agents based on the co-assemblies of **VA**, **AnB** and **RhB-VA**. Nerve agents have been used as chemical warfare agents due to high mammalian toxicity [58]. Upon interacting with diethylchloro-phosphate (DCP) which is a widely used mimic for nerve agents, the dual emissions (**AnB** dominated emission at 423 nm and **RhB-VA** dominated emission at 600 nm) of the co-assemblies decrease with different gradients. Such a selective response (Fig. 5A) enables the ratiometric fluorescent detection of nerve agents in DMF at the micromolar level (Fig. 5B). Because of the solubility decrease caused by reaction of DCP with the oxime group of **VA**

(Supplementary Fig. S10), the aggregation of the co-assemblies is enhanced (Supplementary Fig. S11), contributing to the observed fluorescence quenching. Interestingly, both of the short-wavelength and long-wavelength responses are more sensitive than those observed from the corresponding co-assemblies based on unitary subunits (Fig. 6), indicating a positive combination effect.

Based on a similar fabrication pattern, another ratiometric fluorescent sensing system for saccharides in aqueous solution has been developed. As shown in Fig. 5C, the co-assemblies of **BAB**, **PBI** and **RhB-VA** displays a remarkable ratiometric fluorescence response in the presence of monosaccharides. The emission from **RhB-VA** (at 590 nm) is enhanced greatly while that from **PBI** (at 538 nm) keeps almost unchanged. This is attributed to the fact that binding of saccharide molecules onto the phenylboronic acid side groups (Supplementary Fig. S12) of the HB polymers will sterically prevent the π - π stacking based aggregation of the rhodamine B fluorophores in the sensory co-assemblies. No obvious difference has been observed between the performances of *ortho*-, *meta*- and *para*-**BAB** and the latter was used in the following experiments. DLS experiments reveal that the particle sizes of the co-assemblies only slightly increase after titration with fructose while greatly increase after titration with glucose (Supplementary Fig. S14). This is interpreted by the structural difference that glucose possesses two binding sites for boronic acid while fructose only possesses one [50,59]. That is, crosslinking of the sensory co-assemblies by glucose may occur.

The combination effect of the signalling subunits was also observed in the developed saccharide sensing system. Compared with the remarkable response of the co-assemblies of **BAB**, **PBI** and **RhB-VA**, no obvious fluorescence change has been observed when unitary signalling subunit of **PBI** or **RhB-VA** at the comparable concentration levels was used (Fig. 7). It is also worth noting that the S/R ratio is high in the nerve agent sensing system while it is low in the case of saccharide sensing. For the former system, the high S/R ratio benefits the improvement of the sensitivity by the signal amplification effect. For the latter system, relative higher concentration of recognition subunits is necessary for obtaining a lower detection limit because the formation constants of boronate esters are relatively low (Supplementary Fig. S16). It is clear that, compared with covalent synthesis, our fabrication strategy offer more flexibility and possibility to optimize the sensing performances.

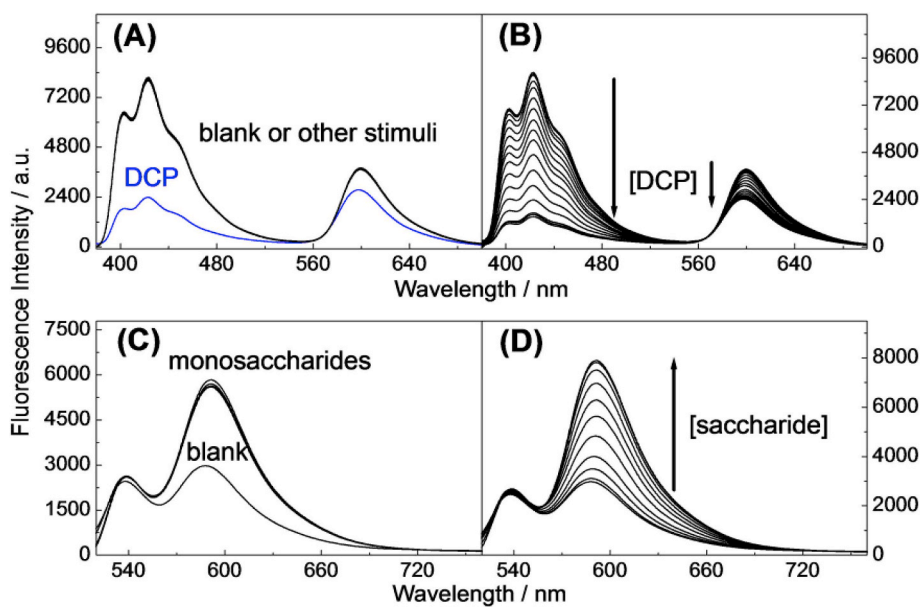


Fig. 5. Fluorescent responses of the investigated sensory assemblies with unitary recognition subunits and binary signalling subunits. (A) Fluorescence responses of the sensory co-assemblies of VA, AnB and RhB-VA in DMF in the presence of different chemical stimuli (100 μM) including DCP, hydrofluoric acid, acetic acid, 4-aminobenzoic acid, benzenesulfonyl chloride and malathion. The concentrations of VA, AnB and RhB-VA were kept at 2.0, 20 and 10 μM , respectively. (B) Fluorescence traces of the sensory co-assemblies of VA, AnB and RhB-VA in DMF upon addition of increasing amount of DCP (from 1.0 μM to 1.0 mM). (C) Fluorescent responses of the sensory co-assemblies of BAB, PBI and RhB-VA to monosaccharides (1.0 mM) including glucose, fructose, galactose and mannose in aqueous solutions buffered at pH 8.0 by 0.02 M $\text{NaH}_2\text{PO}_4\text{-Na}_2\text{HPO}_4$. The concentrations of BAB, PBI and RhB-VA were kept at 12, 8.0 and 4.0 μM , respectively. (D) Fluorescence traces of the sensory co-assemblies of BAB, PBI and RhB-VA upon addition of increasing amount of D-glucose (from 0.2 to 10 mM) in aqueous solutions buffered at pH 8.0 by 0.02 M $\text{NaH}_2\text{PO}_4\text{-Na}_2\text{HPO}_4$. Excitation wavelengths: 371 nm for A and B; 490 nm for C and D.

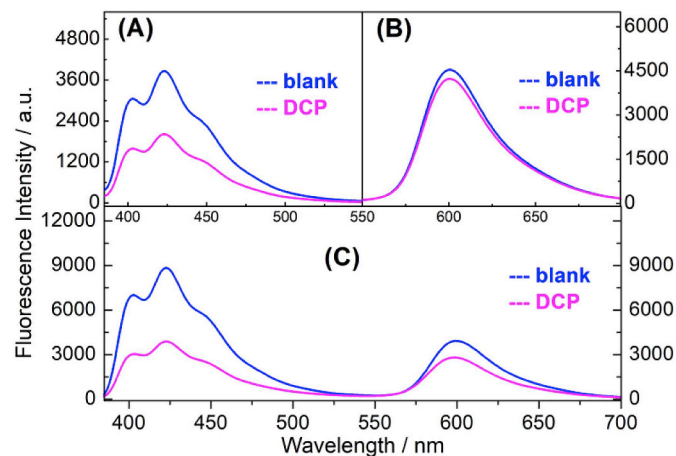


Fig. 6. Comparison of the fluorescence responses of (A) [VA + AnB], (B) [VA + RhB-VA] and (C) [VA + AnB + RhB-VA] sensory co-assemblies to DCP. The concentrations of VA, AnB, RhB-VA and DCP were kept at 2.0, 20, 10 and 100 μM , respectively. $\lambda_{\text{ex}} = 371$ nm.

3.4. Sensory co-assemblies with binary recognition subunits and ternary signalling subunits

It remains greatly challenging to simultaneously monitor multiple targets by single sensor [60,61]. The easy realization of high structural complexity of the developed sensory co-assemblies encourages our attempt to fabricate novel multitarget sensing systems. For the purpose of comparative study, the recognition and signalling subunits including AnB, BAB, PBI and RhB-VA were reorganized under vigorous agitation to form random co-assemblies as a new sensing platform. Upon titration with bisulfite in aqueous solution at pH 7.4, the excimer emission from anthracene (at 497 nm) decreases rapidly and its local emission (at 422 nm) remarkably increases, whereas the RhB-VA dominated emission (at 595 nm) keeps almost unchanged (Fig. 8A). Upon titration with glucose, the AnB dominated dual emissions keep unchanged while the rhodamine B emission is enhanced (Fig. 8B). As previously interpreted, destroying the HB backbones by bisulfite and grafting saccharides onto

the side chains of HB polymers will alleviate the aggregation induced fluorescence quenching of the anthracene and rhodamine B fluorophores, respectively. Upon addition of the mixture of bisulfite and glucose, the dual target-binding interactions result in both enhancements of the short-wavelength and long-wavelength emissions (Fig. 8C). Therefore, simultaneous detection of bisulfite and saccharides can be established based on the short-wavelength and long-wavelength responses accordingly.

Interestingly, the coexistence of bisulfite and glucose induces an additional fluorescence response upon excitation at 490 nm. As shown in Fig. 8D, the PBI-dominated emission (at 540 nm) is enhanced by the dual stimuli, whereas single stimulus of bisulfite or glucose causes no similar response (Supplementary Fig. S18). Both the bisulfite-induced breakage of the HB linkages and the side chain modification by saccharides improve the solubility of the sensory co-assemblies in aqueous solution. The combination of these two factors is able to reduce the serious $\pi\text{-}\pi$ aggregation of PBI fluorophores in the HB networks, therefore explaining the observed fluorescence response. As another proof of the cooperative effect of the two target-binding interactions, the sensitivity of the glucose sensing response is enhanced by the coexistence of bisulfite, probably because the bisulfite-induced breakage of the large co-assemblies will sterically facilitate the saccharide-boronic acid interaction. The above analysis was confirmed by DLS results (Supplementary Fig. S19). The sizes of the sensory aggregates are remarkably decreased by glucose despite the possible occurrence of glucose-induced crosslinking and the coexistence of bisulfite causes a further decrease. Transmission electron microscopy study revealed that the sensory supramolecules were ready to transform into vesicle-like aggregates in reaction with saccharides because of the increasing amphiphaticity (Supplementary Fig. S20).

4. Conclusions

In this work, we developed a general and robust strategy for fabrication of fluorescent sensors. Under a brand-new modularization concept, fluorescent sensory supramolecules can be efficiently formed by HB self-assembly of recognition and signalling subunits. In sharp contrast to traditional covalent fabrication strategy on a case-by-case basis, the subunits can be synthesized independently and interchanged

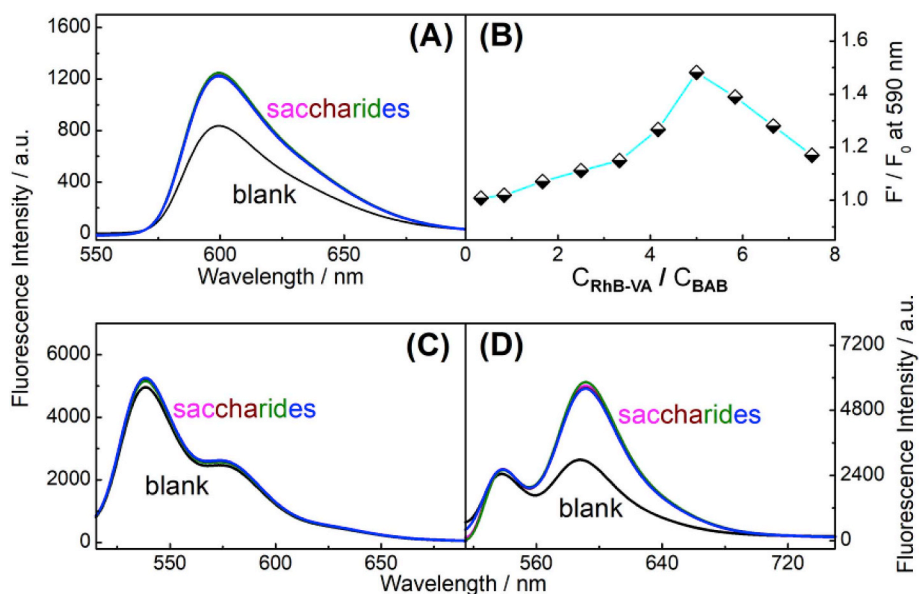


Fig. 7. Comparison of the fluorescence responses of [BAB + RhB-VA], [BAB + PBI] and [BAB + PBI + RhB-VA] sensory co-assemblies to saccharides (1.0 mM, including glucose, fructose, mannose and galactose) upon excitation at 490 nm. The concentrations of BAB and PBI were kept at 12.0 and 8.0 μ M, respectively, in aqueous solutions buffered at pH 8.0 by 0.02 M NaH_2PO_4 - Na_2HPO_4 . (A) Fluorescence responses of [BAB + RhB-VA] ($n_{\text{RhB-VA}}/n_{\text{BAB}} = 5:1$) sensory co-assemblies to saccharides. (B) Influence of the molar ratio of RhB-VA to BAB on the saccharide sensing performance of [BAB + RhB-VA]. (C) Fluorescence responses of [BAB + PBI] sensory co-assemblies to saccharides. (D) Fluorescence responses of [BAB + PBI + RhB-VA] ($n_{\text{BAB}}/n_{\text{PBI}}/n_{\text{RhB-VA}} = 3:2:1$) sensory co-assemblies to saccharides.

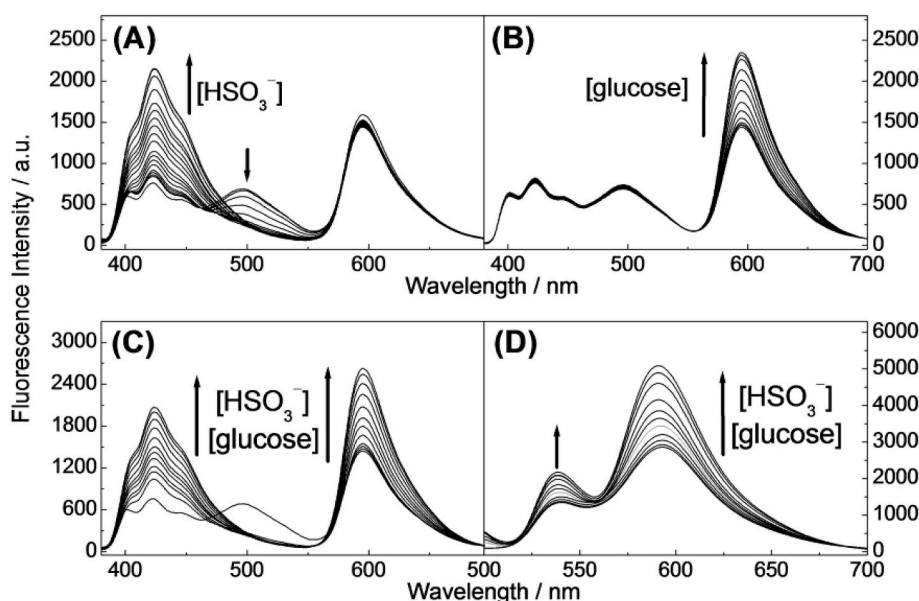


Fig. 8. Fluorescent responses of the sensory co-assemblies AnB, BAB, PBI and RhB-VA upon addition of NaHSO_3 and/or glucose. The concentrations of AnB, BAB, PBI and RhB-VA were kept at 50, 50, 15 and 8.0 μ M, respectively, in $\text{DMF}/\text{H}_2\text{O}$ (3:7, V/V) buffered by 0.02 M NaH_2PO_4 - Na_2HPO_4 . (A) Fluorescence traces upon addition of increasing amount of NaHSO_3 (from 10 μ M to 10 mM). (B) Fluorescence traces upon addition of increasing amount of D-glucose (from 0.10 to 10 mM). (C, D) Fluorescence traces upon addition of increasing amount of the 1:1 mixture of D-glucose and NaHSO_3 (from 0.10 to 10 mM). Excitation wavelengths: 371 nm for A, B and C; 490 nm for D.

between different sensing systems. Furthermore, the numbers, ratios and combination pattern of the subunits can be flexibly modulated to optimize the sensing performances. As proven by the as-developed sensing systems for inorganic ions, gas, chemical warfare agents and bioactive small molecules, our method not only remarkably reduces the synthesis difficulty but also enables the easy realization of advanced functionality of fluorescent sensors.

Acknowledgments

This work was supported by the National Natural Science Foundation of China (21475111, 21775129 and 21435003), and the Fundamental Research Funds for the Central Universities (2011121015).

Appendix A. Supplementary data

Supplementary data to this article can be found online at <https://doi.org/10.1016/j.dyepig.2019.05.011>.

References

- [1] Zhu H, Fan J-L, Du J-J, Peng X-J. Fluorescent probes for sensing and imaging within specific cellular organelles. *Acc Chem Res* 2016;49:2115–26.
- [2] Fernández A, Vendrell M. Smart fluorescent probes for imaging macrophage activity. *Chem Soc Rev* 2016;45:1182–96.
- [3] Sarder P, Maji D, Achilef S. Molecular probes for fluorescence lifetime imaging. *Bioconjug Chem* 2015;26:963–74.
- [4] Schäferling M. The art of fluorescence imaging with chemical sensors. *Angew Chem Int Ed* 2012;51:3532–54.
- [5] Ueno T, Nagano T. Fluorescent probes for sensing and imaging. *Nat Methods* 2011;8:642–5.
- [6] Kobayashi H, Ogawa M, Alford R, Choyke PL, Urano Y. New strategies for fluorescent probe design in medical diagnostic imaging. *Chem Rev* 2010;110:2620–40.
- [7] He L-W, Dong B-L, Liu Y, Lin W-Y. Fluorescent chemosensors manipulated by dual/triple interplaying sensing mechanisms. *Chem Soc Rev* 2016;45:6449–61.
- [8] Lou Z-R, Li P, Han K-L. Redox-responsive fluorescent probes with different design strategies. *Acc Chem Res* 2015;48:1358–68.
- [9] de Silva AP, Gunaratne HQN, Gunnlaugsson T, Huxley AJM, McCoy CP, Rademacher JT, Rice TE. Signaling recognition events with fluorescent sensors and switches. *Chem Rev* 1997;97:515–1566.
- [10] Rasheed T, Bilal M, Nabeel F, Iqbal HMN, Li C-L, Zhou Y-F. Fluorescent sensor based models for the detection of environmentally-related toxic heavy metals. *Sci Total Environ* 2018;615:476–85.
- [11] Wu D, Chen L-Y, Lee W, Ko G, Yin J, Yoon J. Recent progress in the development of

- organic dye based near-infrared fluorescence probes for metal ions. *Coord Chem Rev* 2018;354:74–97.
- [12] Sfrassetto GT, Satriano C, Tomaselli GA, Rizzarelli E. Synthetic fluorescent probes to map metallothionein and intracellular fate of zinc and copper. *Coord Chem Rev* 2011;311:125–67.
- [13] Aron AT, Ramos-Torres KM, Cotruvo Jr. JA, Chang CJ. Recognition- and reactivity-based fluorescent probes for studying transition metal signaling in living systems. *Acc Chem Res* 2015;48:2434–42.
- [14] Kim HN, Ren WX, Kim JS, Yoon J. Fluorescent and colorimetric sensors for detection of lead, cadmium, and mercury ions. *Chem Soc Rev* 2012;41:3210–44.
- [15] Domaille DW, Que EL, Chang CJ. Synthetic fluorescent sensors for studying the cell biology of metals. *Nat Chem Biol* 2008;4:168–75.
- [16] Ashton TD, Jolliffe KA, Pfeffer FM. Luminescent probes for the bioimaging of small anionic species *in vitro* and *in vivo*. *Chem Soc Rev* 2015;44:4547–95.
- [17] Aletti AB, Gillen DM, Gunnlaugsson T. Luminescent/colorimetric probes and (chemo-) sensors for detecting anions based on transition and lanthanide ion receptor/binding complexes. *Coord Chem Rev* 2018;354:98–120.
- [18] Zhang D-W, Cochrane JR, Martinez A, Gao G-H. Recent advances in $H_2PO_4^-$ fluorescent sensors. *RSC Adv* 2014;4:29735–49.
- [19] Martínez-Mañez R, Sancenón F. Fluorogenic and chromogenic chemosensors and reagents for anions. *Chem Rev* 2013;103:4419–76.
- [20] Strianese M, Pellicchia C. Metal complexes as fluorescent probes for sensing biologically relevant gas molecules. *Coord Chem Rev* 2016;318:16–28.
- [21] Marín-Hernández C, Toscani A, Sancenón F, Wilton-Ely JDET, Martínez-Mañez R. Chromo-fluorogenic probes for carbon monoxide detection. *Chem Commun* 2016;52:5902–11.
- [22] Li H-L, Wan A-J. Fluorescent probes for real-time measurement of nitric oxide in living cells. *Analyst* 2015;140:7129–41.
- [23] Kumar N, Bhalla V, Kumar M. Recent developments of fluorescent probes for the detection of gasotransmitters (NO, CO and H_2S). *Coord Chem Rev* 2013;257:2335–47.
- [24] Lin VS, Chang CJ. Fluorescent probes for sensing and imaging biological hydrogen sulphide. *Curr Opin Chem Biol* 2012;16:595–601.
- [25] McQuade LE, Lippard SJ. Fluorescent probes to investigate nitric oxide and other reactive nitrogen species in biology. *Curr Opin Chem Biol* 2010;14:43–9.
- [26] Jiao X-Y, Li Y, Niu J-Y, Xie X-L, Wang X, Tang B. Small-molecule fluorescent probes for imaging and detection of reactive oxygen, nitrogen, and sulfur species in biological systems. *Anal Chem* 2018;90:533–55.
- [27] Andina D, Leroux J-C, Luciani P. Ratiometric fluorescent probes for the detection of reactive oxygen species. *Chem Eur J* 2017;23:13549–73.
- [28] Chen X-Q, Wang F, Hyun JY, Wei T-W, Qiang J, Ren X-T, Shin I, Yoon J. Recent progress in the development of fluorescent, luminescent and colorimetric probes for detection of reactive oxygen and nitrogen species. *Chem Soc Rev* 2016;45:2976–3016.
- [29] Wang H-S. Development of fluorescent and luminescent probes for reactive oxygen species. *Trends Anal Chem* 2016;85:181–202.
- [30] Chen X-Q, Tian X-Z, Shin I, Yoon J. Fluorescent and luminescent probes for detection of reactive oxygen and nitrogen species. *Chem Soc Rev* 2011;40:4783–804.
- [31] Chin J, Kim H-J. Near-infrared fluorescent probes for peptidases. *Coord Chem Rev* 2018;354:169–81.
- [32] Yin C-X, Xiong K-M, Huo F-J, Salamanca JC, Strongin RM. Fluorescent probes with multiple binding sites for the discrimination of Cys, Hcy, and GSH. *Angew Chem Int Ed* 2017;56:13188–98.
- [33] Bi A-Y, Yang S-Q, Liu M, Wang X-B, Liao W-H, Zeng W-B. Fluorescent probes and materials for detecting formaldehyde: from laboratory to indoor for environmental and health monitoring. *RSC Adv* 2017;7:36421–32.
- [34] Yoshihara T, Hirakawa Y, Hosaka M, Nangaku M, Tobita S. Oxygen imaging of living cells and tissues using luminescent molecular probes. *J Photochem Photobiol, A C* 2017;30:71–95.
- [35] Fernández A, Vendrell M. Smart fluorescent probes for imaging macrophage activity. *Chem Soc Rev* 2016;45:1182–96.
- [36] Bruemmer KJ, Brewer TF, Chang CJ. Fluorescent probes for imaging formaldehyde in biological systems. *Curr Opin Chem Biol* 2017;39:17–23.
- [37] Chen H, Tang Y-H, Lin W-Y. Recent progress in the fluorescent probes for the specific imaging of small molecular weight thiols in living cells. *Trends Anal Chem* 2017;76:166–81.
- [38] Niu L-Y, Chen Y-Z, Zheng H-R, Wu L-Z, Tung C-H, Yang Q-Z. Design strategies of fluorescent probes for selective detection among biothiols. *Chem Soc Rev* 2017;46:6143–60.
- [39] Suzuki Y, Yokoyama K. Development of functional fluorescent molecular probes for the detection of biological substances. *Biosensors* 2015;5:337–63.
- [40] Li W-H, Li D-L. Fluorescent probes for monitoring regulated secretion. *Curr Opin Chem Biol* 2013;17:672–81.
- [41] Cao H-S, Heagy MD. Fluorescent chemosensors for carbohydrates: a decade's worth of bright spies for saccharides in review. *J Fluoresc* 2004;14:569–84.
- [42] Prins LJ, Reinhoudt DN, Timmerman P. Noncovalent synthesis using hydrogen bonding. *Angew Chem Int Ed* 2001;40:2382–426.
- [43] Gruber B, Stadlbauer S, Späth A, Weiss S, Kalinina M, König B. Modular chemosensors from self-assembled vesicle membranes with amphiphilic binding sites and reporter dyes. *Angew Chem Int Ed* 2010;49:7125–8.
- [44] Whitesides GM, Simanek EE, Mathias JP, Seto CT, Chin DN, Mammen M, Gordon DM. Noncovalent synthesis: using physical-organic chemistry to make aggregates. *Acc Chem Res* 1995;28:37–44.
- [45] Sherrington DC, Taskinen KA. Self-assembly in synthetic macromolecular systems via multiple hydrogen bonding interactions. *Chem Soc Rev* 2001;30:83–93.
- [46] Yagai S. Supramolecular complexes of functional chromophores based on multiple hydrogen-bonding interactions. *J Photochem Photobiol, A C* 2006;7:164–82.
- [47] Wilson AJ. Non-covalent polymer assembly using arrays of hydrogen-bonds. *Soft Matter* 2007;3:409–25.
- [48] Wang J-N, Zhang L, Qi Q-Q, Li S-H, Jiang Y-B. Specific ratiometric fluorescent sensing of Hg^{2+} via the formation of mercury(II) barbiturate coordination polymers. *Anal Methods* 2013;5:608–11.
- [49] Bull SD, Davidson MG, van Denelsen JMH, Fossey JS, Jenkins ATA, Jiang Y-B, Kubo Y, Marken F, Sakurai K, Zhao J-Z, James TD. Exploiting the reversible covalent bonding of boronic acids: recognition, sensing, and assembly. *Acc Chem Res* 2013;46:312–26.
- [50] Wu X, Li Z, Chen X-X, Fossey JS, James TD, Jiang Y-B. Selective sensing of saccharides using simple boronic acids and their aggregates. *Chem Soc Rev* 2013;42:8032–48.
- [51] Gupta RC. *Handbook of toxicology of chemical warfare agents*. San Diego: Elsevier; 2009. p. 985–96.
- [52] Chen Z-H, Deng S-B, Wei H-R, Wang B, Huang J, Yu G. Activated carbons and amine-modified materials for carbon dioxide capture — a review. *Front Environ Sci Eng* 2013;7:326–40.
- [53] Alexis N, Barnes C, Bernstein IL, Bernstein JA, Nel A, Peden D, Diaz-Sanchez D, Tarlo SM, Williams PB. Health effects of air pollution. *J Allergy Clin Immunol* 2004;114:1116–23.
- [54] Liu D, Jin H, Tang C, Du J. Sulfur dioxide: a novel gaseous signal in the regulation of cardiovascular functions. *Mini Rev Med Chem* 2010;10:1039–45.
- [55] Zhang R-Q, Yan F-Y, Huang Y-C, Kong D-P, Ye Q-H, Xu J-X, Chen L. Rhodamine-based ratiometric fluorescent probes based on excitation energy transfer mechanisms: construction and applications in ratiometric sensing. *RSC Adv* 2016;6:50732–60.
- [56] Lee MH, Kim JS, Sessler JL. Small molecule-based ratiometric fluorescence probes for cations, anions, and biomolecules. *Chem Soc Rev* 2015;44:4185–91.
- [57] Yuan L, Lin W-Y, Zheng K-B, Zhu S-S. FRET-based small-molecule fluorescent probes: rational design and bioimaging applications. *Acc Chem Res* 2013;46:1462–73.
- [58] Kim K, Tsay OG, Atwood DA, Churchill DG. Destruction and detection of chemical warfare agents. *Chem Rev* 2011;111:5345–403.
- [59] Liu Y, Deng C-M, Tang L, Qin A-J, Hu R-R, Sun JZ, Tang BZ. Specific detection of D-glucose by a tetraphenylethene-based fluorescent sensor. *J Am Chem Soc* 2011;133:660–3.
- [60] Stich MJ, Fischer LH, Wolfbeis OS. Multiple fluorescent chemical sensing and imaging. *Chem Soc Rev* 2010;39:3102–14.
- [61] You L, Zha D-J, Anslyn EV. Recent advances in supramolecular analytical chemistry using optical sensing. *Chem Rev* 2015;115:7840–92.